Electronic structure of the magnetic halide double perovskites Cs₂(Ag, Na)FeCl₆ from first principles

Johan Klarbring [1,*] Utkarsh Singh [1] Sergei I. Simak,[1,2] and Igor A. Abrikosov [1]

[1]*Theoretical Physics Division, Department of Physics, Chemistry and Biology (IFM), Linköping University, SE–581 83, Linköping, Sweden*
[2]*Department of Physics and Astronomy, Uppsala University, SE–75120 Uppsala, Sweden*

A family of magnetic halide double perovskites (HDPs) have recently attracted attention due to their potential to broaden application areas of halide double perovskites into, e.g., spintronics. Up to date the theoretical modeling of these systems have relied on primitive approximations to the density functional theory (DFT). In this paper, we study structural, electronic and magnetic properties of the Fe^{3+}-containing HDPs $Cs_2AgFeCl_6$ and $Cs_2NaFeCl_6$ using a combination of more advanced DFT-based methods, including $DFT + U$, hybrid-DFT, and treatments of various magnetic states. We examine the effect of varying the effective Hubbard parameter, U_{eff}, in $DFT + U$ and the mixing-parameter, α, in hybrid DFT on the electronic structure and structural properties. Our results reveal a set of localized Fe(d) states that are highly sensitive to these parameters. $Cs_2AgFeCl_6$ and $Cs_2NaFeCl_6$ are both antiferromagnets with Neél temperatures well below room temperature and are thus in their paramagnetic (PM) state at the external conditions relevant to most applications. Therefore, we have examined the effect of disordered magnetism on the electronic structure of these systems and find that while $Cs_2NaFeCl_6$ is largely unaffected, $Cs_2AgFeCl_6$ shows significant renormalization of its electronic band structure.

I. INTRODUCTION

Research into metal halide perovskite (MHP) semiconductors has steadily increased over the last decade to where it is currently one of the most active fields in materials science [1]. While lead-containing MHPs have been at the forefront of this research, a number of lead-free derivatives have emerged as interesting alternatives [2]. These subclasses often aim to address deficiencies, not just related to the toxicity of lead, but also in terms of poor stability of several MHPs. The so-called lead-free halide double perovskites (HDPs), where the Pb^{2+} ions are replaced with a pair of mono and trivalent cations, is one such class of materials which has emerged over the last years [3].

Recently, a set of Fe^{3+}-based HDPs, including $Cs_2NaFeCl_6$ and $Cs_2AgFeCl_6$, have garnered attention [4–6]. While $Cs_2NaFeCl_6$ was synthesized at least as early as 1976 [7], renewed attention has been gained just in the last few years. In addition to $Cs_2NaFeCl_6$ and $Cs_2AgFeCl_6$, related alloys have also been synthesized [6]. These systems contain magnetic Fe^{3+} ions with a $3d^5$ electronic configuration and initial experiments indicate that they are in their high-spin (HS) configuration, yielding a large magnetic moment [8].

As such, an associated set of physical phenomena related to their magnetism become of relevance. $Cs_2NaFeCl_6$ and $Cs_2AgFeCl_6$ both crystallize in the ideal cubic double perovskite structure with space group $Fm\bar{3}m$ (No. 225) at ambient conditions, see Fig. 1. They are further found to be antiferromagnets (AFM) with low Néel temperatures of 3 K and 18 K, respectively [8]. As such, they are both deep in their paramagnetic (PM) states at ambient conditions.

The presence of the partially filled $3d$ shell differentiates $Cs_2NaFeCl_6$ and $Cs_2AgFeCl_6$ from the majority of MHPs studied in the literature. These Fe($3d$) states are expected to be highly localized and an accurate treatment typically requires consideration beyond standard semilocal DFT. In this work, we explore two such approaches. The first is the $DFT + U$ method [9], where an (effective) onsite Hubbard term, U_{eff}, is added to the effective Kohn-Sham potential of the localized states. This method is advantageous in that it adds negligible computational effort compared to standard semilocal DFT. However, a choice needs to be made on the value of the effective U_{eff} parameter. While this can, in principle, be estimated from first principles [10], often a value is taken to match some experimentally determined property. The second approach is hybrid DFT, where a fraction of exact exchange is mixed in with the semilocal DFT exchange. This approach is often chosen for semiconductors and insulators when accurate electronic structures are desired. Although it acts in a similar way to $DFT + U$ on highly localized states [11], it is not as popular for studies of such systems. Computationally, hybrid DFT is significantly more expensive than $DFT + U$ and suffers from a similar problem as $DFT + U$ when it comes to choosing the amount, α, of exact exchange to mix in.

---

*johan.klarbring@liu.se

A second challenge in modeling these systems, also rarely encountered for MHPs, is that they are in the PM state at the relevant external conditions. The PM state is sometimes modeled as nonmagnetic, without the presence of local magnetic moments, which could lead to erroneous conclusions [12].

Previous DFT studies on $Cs_2NaFeCl_6$ and $Cs_2AgFeCl_6$ [4,13,14] have either been performed with a NM or FM state and have not directly addressed the issue of the modeling of the strongly localized Fe(d) states. In the current paper, we therefore aim to explore how DFT $+ U$ and hybrid-DFT behave in modeling these systems and study the influence of varying values of U and the mixing parameter, α, respectively. Moreover, we use a description of the PM state in the framework of the disordered local moment (DLM) picture [15], using a DLM-supercell approach [16] to explore how the disordered PM state influences structural and electronic structure properties.

II. COMPUTATIONAL DETAILS

All computations were performed using plane-wave Kohn-Sham DFT and the PAW method [17] as implemented in VASP [18–20]. We have used the PBEsol [21] form of the exchange-correlation functional augmented with an effective on-site U_{eff} correction on the Fe(d) states in the form according to Dudarev *et al.* [22], as well as range-separated hybrid DFT [23] with varying values of the mixing-parameter α. For the majority of the calculations we have used a 450 eV cutoff energy, an $8 \times 8 \times 8$ sampling of the first Brillouin zone (BZ) of the 10 atom primitive unit cell, a 10^{-6} eV convergence criterion for the self-consistent field (SCF) cycles and the "PREC = Accurate" mode in VASP. Full structural relaxations (lattice vectors and internal coordinates) were performed until all the atomic forces were < 5 meV/Å. For relaxations with hybrid-DFT we have used a less dense $4 \times 4 \times 4$ k-point grid. We confirmed that yielded forces < 6 meV/Å different compared with the $8 \times 8 \times 8$ grid used for calculations of densities of states (DOS). The employed PAW potentials treated the Cs($5s5p6s$), Ag($4d5s$), Na($2p3s$), Fe($3p3d4s$), and Cl($3s3p$) states as valence. Details on chemical bonding was obtained from a Crystal Orbital Hamiltonian Population (COHP) [24] analysis, using the LOBSTER [25–27] package.

The PM state was modeled with special quasirandom structure (SQS) [28] distributions of the spin-up and spin-down Fe magnetic moments in a disordered-local moment (DLM) fashion [16]. For the calculations of energies of different magnetic states we used a 320 atom supercell, constructed as a $2 \times 2 \times 2$ repetition of the 40 atom conventional cubic unit cell. We relaxed the structures using Γ point BZ sampling and then evaluated the total energies on this relaxed geometry using a $2 \times 2 \times 2$ k-point grid. Effective band structures (EBS) in the BZ of the primitive unit cell were obtained using band unfolding [29] as implemented in the BandUP code [30]. For these calculations we used a $4 \times 4 \times 4$ supercell of the primitive fcc unit cell (640 atoms). In order to make these calculations computationally feasible, the accuracy settings were slightly reduced as follows: cutoff energy 300 eV, energy convergence criterion 10^{-5} eV, and "*PREC = Normal*." We have recalculated the band structures of the FM unit cell with

these settings to confirm that band structures agree almost within the width of the line in the displayed band structures.

III. RESULTS

A. Basic electronic and structural properties

We start by examining the structural and magnetic properties, as well as the electronic structure of $Cs_2NaFeCl_6$ and $Cs_2AgFeCl_6$ across a range of U_{eff} and α values. Although, as mentioned in the introduction, $Cs_2NaFeCl_6$ and $Cs_2AgFeCl_6$ are both AFM at low temperature and in their disordered PM state at relevant external conditions, in this section we will primarily treat them in their ferromagnetic (FM) state. This allows us to retain the symmetry of the double perovskite structure and to most easily highlight basic features of their electronic structure. The effect of different magnetic states on the electronic structure will then be considered in more detail in Sec. III B.

The double perovskite structure contains two degrees of freedom: the lattice parameter a (or equivalently the unit cell volume) and the position of the Cl atom along the (Ag/Na)-Cl-Fe bond. Table I lists these parameters for both $Cs_2NaFeCl_6$ and $Cs_2AgFeCl_6$ for different U values in PBEsol $+ U$ and different α values in the HSE methodology. To assess the importance of the magnetic state on the structural parameters, we show results for the FM, PM, and NM states in the case of $U_{\mathrm{eff}} = 3$ eV.

Generally, PBEsol $+ U$ gives the better structural parameters in comparison to experiments, with HSE somewhat overestimating lattice constants. The structural parameters are rather weakly influenced by varying the values of U_{eff} and α. It is, however, interesting to note that increasing U_{eff} increases the Fe-Cl bond length and lattice constant, while increasing α instead decreases the same bond length and lattice constant. We can also see from Table I that, while the NM calculations clearly give erroneous results for the lattice constant and bond lengths, the precise nature of the magnetic state, i.e., FM or PM, is not influential on the structural parameters, as long as local magnetic moments are included in the calculations.

Table I also shows the total magnetic moment in the unit cell and the local magnetic moments on the Fe atoms for different values of U_{eff} and α [31]. We see that in all cases, expect for $U = 0$ eV in $Cs_2AgFeCl_6$, there is a total magnetic moment of 5 μ_B in the unit cell, as expected from the five unpaired electrons of HS Fe^{3+}. The local magnetic moment on the Fe ions increases for increasing U_{eff} (or α), due to the increased charge localization.

Turning to the electronic structure, Fig. 2 shows the densities of states (DOS) in the FM spin configuration for $Cs_2NaFeCl_6$, with U_{eff} values on the Fe 3d states varying from 0 to 6 eV.

The most eye-catching feature of the DOS is the highly localized Fe-d states. These separate, as dictated by the octahedral coordination environment given by the Cl-p ligands, into states with e_g and t_{2g} symmetry. In a simple picture, the e_g and t_{2g} orbitals have both Coulomb and covalent interactions with the ligands. The e_g orbitals point more directly toward the ligands and the Coulomb repulsion is thus stronger than for the t_{2g} orbitals, but the covalent interaction also tends to be larger.

TABLE I. Lattice constant, a and select bondlengths (in units of Å); total magnetic moments in the unit cell, $\mu(uc)$; and local magnetic moments on the Fe^{3+}-ion, $\mu(Fe)$. For the PM states, the average values of the bond lengths and $\mu(Fe)$ are given. Experimental results are from Refs. [4,5].

		$Cs_2NaFeCl_6$				
Method	Magnetic state	a	d(Fe-Cl)	d(Na-Cl)	$\mu(uc)$	$\mu(Fe)$
Experiment (80 K) [5]	PM	10.2591	2.366	2.764		
PBEsol + U						
$U = 0$ eV	FM	10.246	2.377	2.746	5.00	3.88
$U = 3$ eV	FM	10.258	2.381	2.747	5.00	4.06
	NM	10.073	2.276	2.761	0	0
	PM	10.258	2.381	2.748	–	4.06
$U = 6$ eV	FM	10.266	2.385	2.748	5.00	4.22
$U = 9$ eV	FM	10.271	2.388	2.748	5.00	4.38
HSE						
$\alpha = 0.125$	FM	10.461	2.407	2.823	5.00	4.04
$\alpha = 0.250$	FM	10.432	2.399	2.817	5.00	4.16
$\alpha = 0.375$	FM	10.397	2.392	2.807	5.00	4.26
		$Cs_2AgFeCl_6$				
Method	Magnetic state	a	d(Fe-Cl)	d(Na-Cl)	$\mu(uc)$	$\mu(Fe)$
Experiment (300 K) [4]	PM	10.2023	2.382	2.719		
PBEsol + U						
$U = 0$ eV	FM	10.079	2.387	2.652	4.53	3.67
$U = 3$ eV	FM	10.126	2.396	2.667	5.00	4.01
	NM	9.93	2.295	2.668	0	0
	PM	10.116	2.381	2.747	–	4.06
$U = 6$ eV	FM	10.139	2.400	2.669	5.00	4.16
$U = 9$ eV	FM	10.150	2.402	2.673	5.00	4.32
HSE						
$\alpha = 0.125$	FM	10.377	2.416	2.773	5.00	4.01
$\alpha = 0.250$	FM	10.364	2.405	2.778	5.00	4.13
$\alpha = 0.375$	FM	10.348	2.395	2.779	5.00	4.24

In general, increasing the value of U_{eff} has the effect of driving the occupied and unoccupied states to which the U_{eff} is applied, Fe $3d$ states in our case, down and up in energy, respectively. This can clearly be seen to be the case for $Cs_2NaFeCl_6$ in Fig. 2. Importantly, however, the sharper t_{2g}
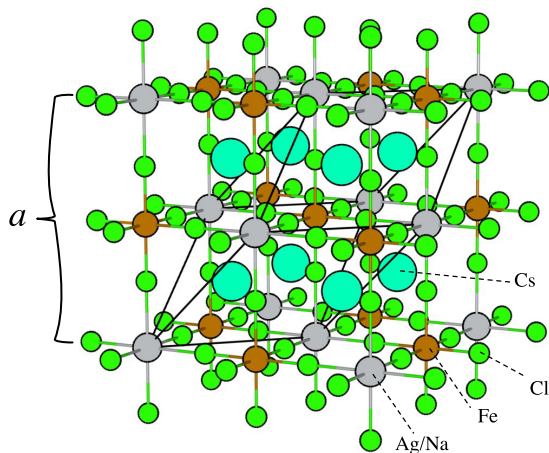

FIG. 1. Illustration of the double perovskite structure in the conventional cubic representation. The black lines mark the primitive fcc unit cell and a denotes the lattice constant.

and the broader e_g states move with U_{eff} at different rates. This is particularly true for the unoccupied e_g/t_{2g} states, where the t_{2g} states are initially lower in energy, but where a crossing with the e_g states happens at $U_{eff} \approx 6$ eV. This is because the e_g states have, as mentioned above, a stronger covalent interaction with the ligands and as such have a counteracting effect to the increase in U_{eff}, while the more localized t_{2g} states move with U_{eff} at will.

There are two sets of Fe(d)-Cl(p) hybridized states in each spin channel, one with predominantly Fe(d) character and one with predominantly Cl(p) character. In the majority spin channel both sets are occupied, while the predominantly Fe(d) states are unoccupied in the minority spin channel. We see that the predominantly Fe(d) peaks corresponding to occupied e_g and t_{2g} states and unoccupied t_{2g} states are very sharp, while the unoccupied e_g band is more dispersed.

To get further insight into the electronic structure of $Cs_2NaFeCl_6$, Fig. 3 shows the DOS for $U_{eff} = 3$ eV, along with the Fe-Cl partial crystal orbital Hamiltonian population (COHP). Analyzing the Fe($3d$)-Cl($3p$) hybridized states, we see that the predominantly Fe(d) peaks are of bonding and antibonding character in the majority and minority spin channels, respectively, and that the order of the t_{2g} and e_g states is opposite in the two spin channels. The predominantly Cl(p) states are instead antibonding in the majority
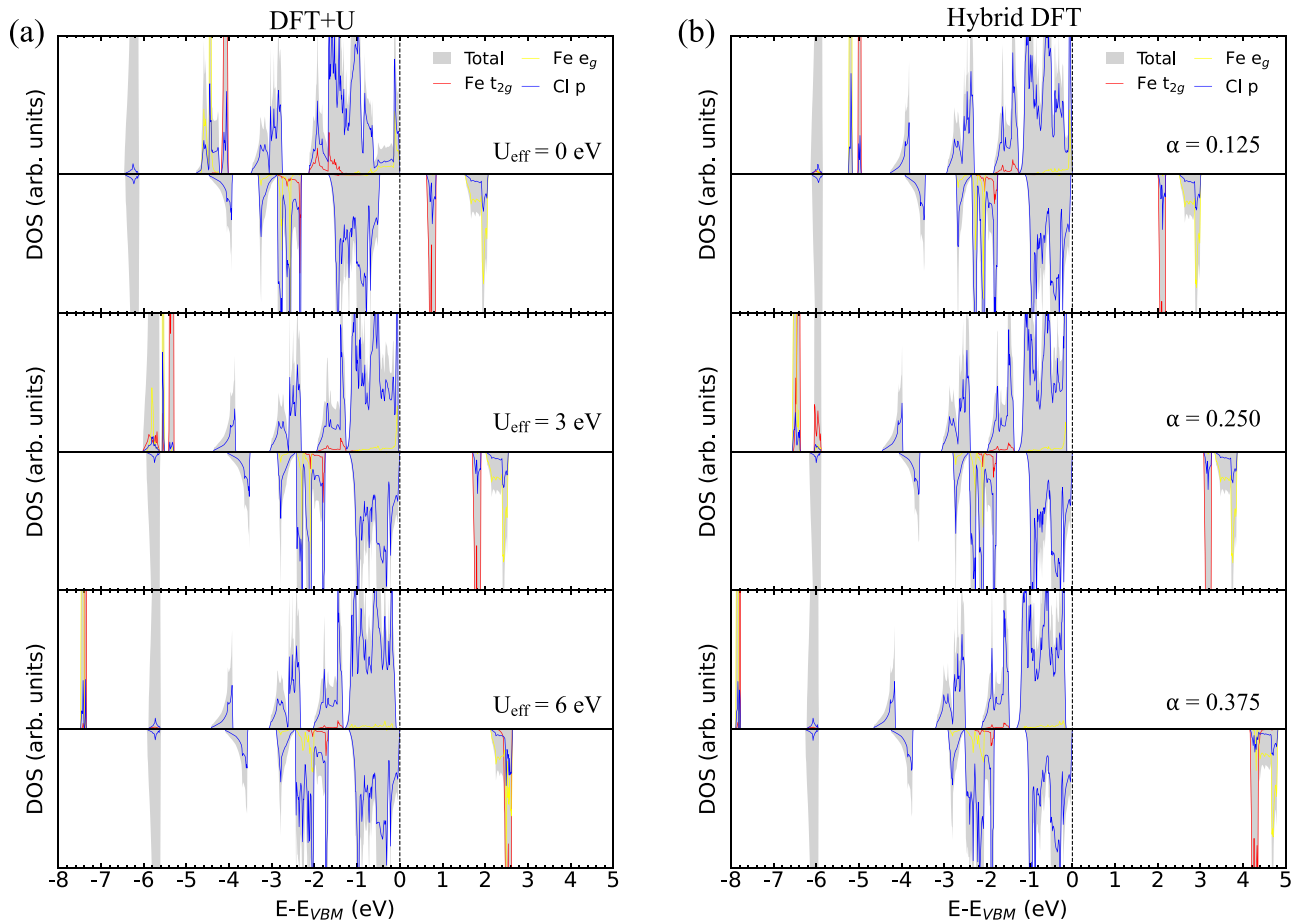
FIG. 2. Electronic DOS for $Cs_2NaFeCl_6$ in the FM state, for (a) varying values of U_{eff} on the Fe(d) states in the PBEsol $+ U$ methodology and (b) varying values of α in the hybrid DFT (default HSE06 range separation parameter). The DOS are aligned to the VBM. The unmarked peak at around -6 eV corresponds to Cs(p) states.

and bonding in the minority spin channel. As expected, the bonding-antibonding energy splitting is larger for the e_g orbitals, resulting in the opposite order of t_{2g}/e_g states for the bonding and antibonding Fe(3d)-Cl(3p) combinations for lower values of U_{eff}.

Increasing the value of U_{eff} has the additional effect of localizing the Fe-d states and thus reducing the covalent interaction with the ligands. The impact of this is seen most clearly for the Fe(3d)-Cl(3p) antibonding states in the majority spin channel where, upon increasing U_{eff} the Fe(e_g/t_{2g}) weight rapidly decreases and gets redistributed into the sharp bonding states. In fact, the effect of adding U_{eff} is rather drastic on the top of the valence band; for $U_{eff} = 0$ eV, antibonding Fe(e_g)-Cl(p) states are separated out from the rest of the VB in the majority spin channel. This is a clear indication that "regular" semilocal DFT functionals, such as PBEsol, do not accurately describe the electronic structure of $Cs_2NaFeCl_6$.

As can be seen in Fig. 2(b), the effect of increasing the mixing parameter α has similar impact on the Fe(d) states as increasing U_{eff}. This is to be expected as DFT $+ U$ and hybrid DFT can be shown to behave very similarly for localized states [11]. An important difference, however, is that the unoccupied t_{2g} states move up in energy on increasing U_{eff} at a much larger rate than the e_g states, this rate difference is much smaller on increasing α. Indeed, the unoccupied t_{2g} states stay below the

e_g states at least up to $\alpha = 0.5$. This difference in behavior could be related to different spatial localization in hybrid DFT and DFT $+ U$ calculations, resulting in somewhat different splitting between Coulomb and covalent interactions [32].

Another interesting observation is that the sharp occupied bonding Fe(e_g)-Cl(p) states are lower in energy than the t_{2g} states. This is contrary to the predictions from simple crystal field theory (CFT) applied to an octahedral coordination environment, where the opposite ordering of t_{2g} and e_g states is expected. Indeed, if the atomic d orbitals are split simply by their Coulomb interaction with the ligands, represented as negative point charges, the e_g orbitals have to lie above the t_{2g} orbitals. This is, as mentioned above, because e_g orbitals point more directly toward the ligands and are thus repelled more strongly. However, moving beyond CFT and also considering covalent interactions between the e_g/t_{2g} orbitals and the ligands, things are a bit less straightforward.

For the typical case where the transition metal (TM) d orbitals lie above the ligand p levels, the antibonding combination of ligand p and TM d are the ones which are predominately of TM d character and which are often referred to as just the TM d states. These states also show the "normal" order of e_g/t_{2g} orbitals [33]. However, in the opposite case where the TM d lie below the ligand p levels, the predominantly d levels are the bonding orbitals which can show the
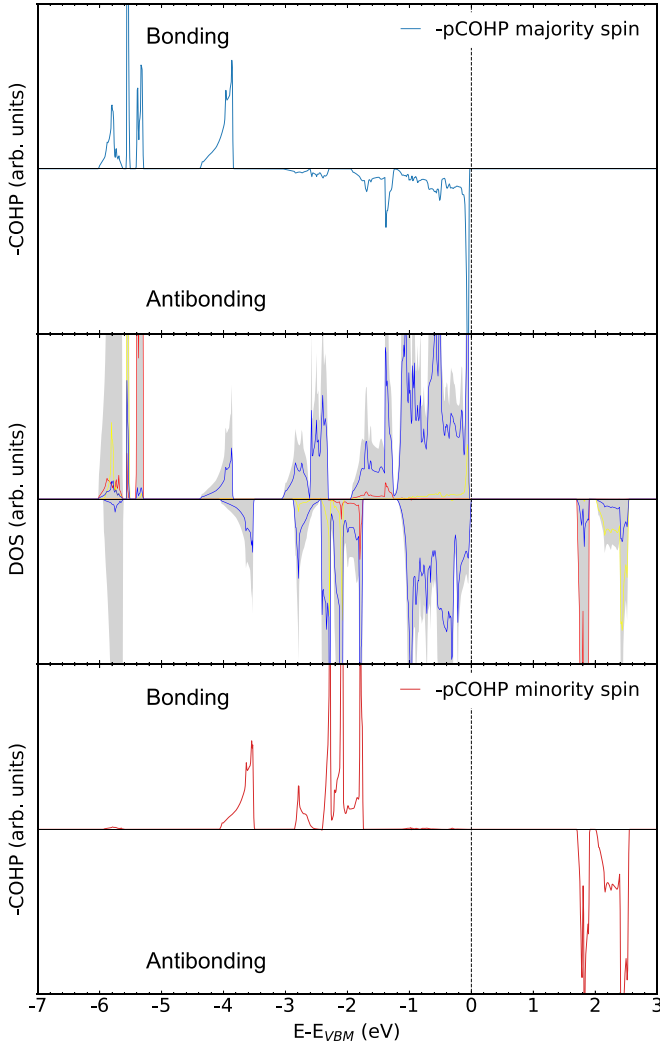
FIG. 3. PBEsol $+ U (3 \text{ eV})$ DOS (middle panel) and corresponding Fe-Cl partial COHP (pCOHP) for the majority (blue line, top panel) and minority (red line, bottom panel) spin channels. Positive and negative values of $-$pCOHP correspond to bonding and antibonding states, respectively. The bonding states around -4 eV are of Fe(s)-Cl(p) character. The large, unmarked, peak at around -6 eV corresponds to Cs(p) states.

FIG. 4. Schematic illustration of Fe(d)-Cl(p) hybridization in $Cs_2NaFeCl_6$. Yellow and blue boxes indicate states of predominately Fe(d) and Cl(p) character, respectively.

between Fe^{3+}, and is responsible for the different magnetic energetics in $Cs_2AgFeCl_6$ compared to $Cs_2NaFeCl_6$.

It is worth noting that for $U_{eff} = 0$ eV, the states at the top of the valence band in the majority spin channel overlap in energy with the sharp Fe(t_{2g}) peak in the minority spin channel, resulting essentially in a metallic system.

B. Magnetic states

While the initial investigation in the previous section was, for clarity and simplicity, done primarily with a FM spin-configuration of the Fe atoms, experiments indicate that both $Cs_2NaFeCl_6$ and $Cs_2AgFeCl_6$ have AFM groundstates with low Néel temperatures [8]. Table II lists the total energies of the FM, PM, and three different AFM [34] spin configurations. The calculations used PBEsol $+ U (3 \text{ eV})$; This U_{eff} was chosen since it gives the same ordering of the unoccupied e_g/t_{2g} states as hybrid DFT for reasonable values of α. The lattice constant was fixed at its relaxed value in the FM state while internal degrees of freedom were relaxed for each magnetic state.

We see that the lowest energy configuration is AFM in both cases, in agreement with the experimental results that these systems are AFM at low temperatures [8]. The energy

opposite t_{2g}/e_g ordering. In the present case, we propose that the Fe($3d$) and Cl($3p$) hybridization in $Cs_2NaFeCl_6$ can be schematically illustrated as in Fig. 4.

Figure 5 shows the DOS for different U_{eff} and α for $Cs_2AgFeCl_6$, which is, in many ways, similar to $Cs_2NaFeCl_6$. Indeed, the Fe(e_g/t_{2g}) states behave in much the same way, the primary difference being that the unoccupied e_g band is broader in $Cs_2AgFeCl_6$ than in $Cs_2NaFeCl_6$. This is due to a stronger Fe-Fe interaction, as will be discussed further below. The main difference between the two systems, however, is the presence of Ag(d) states in the main valence band. In particular, bands of predominantly Ag(e_g)-Cl(p) character are at the top of the valence band in the majority spin channel. It is thus clear that beside the Fe^{3+}-ions, the Ag^+ ions are also spinpolarized, despite the fact that the they have a full d^{10} electron configuration. As we will see below, these Ag(e_g) states are important in mediating the magnetic interaction
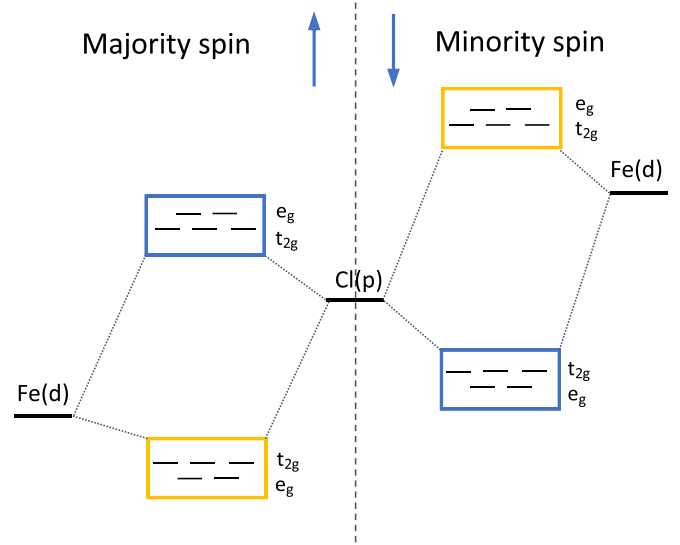
TABLE II. Energies of different magnetic states, referenced to the FM configuration in $Cs_2NaFeCl_6$ and $Cs_2AgFeCl_6$.

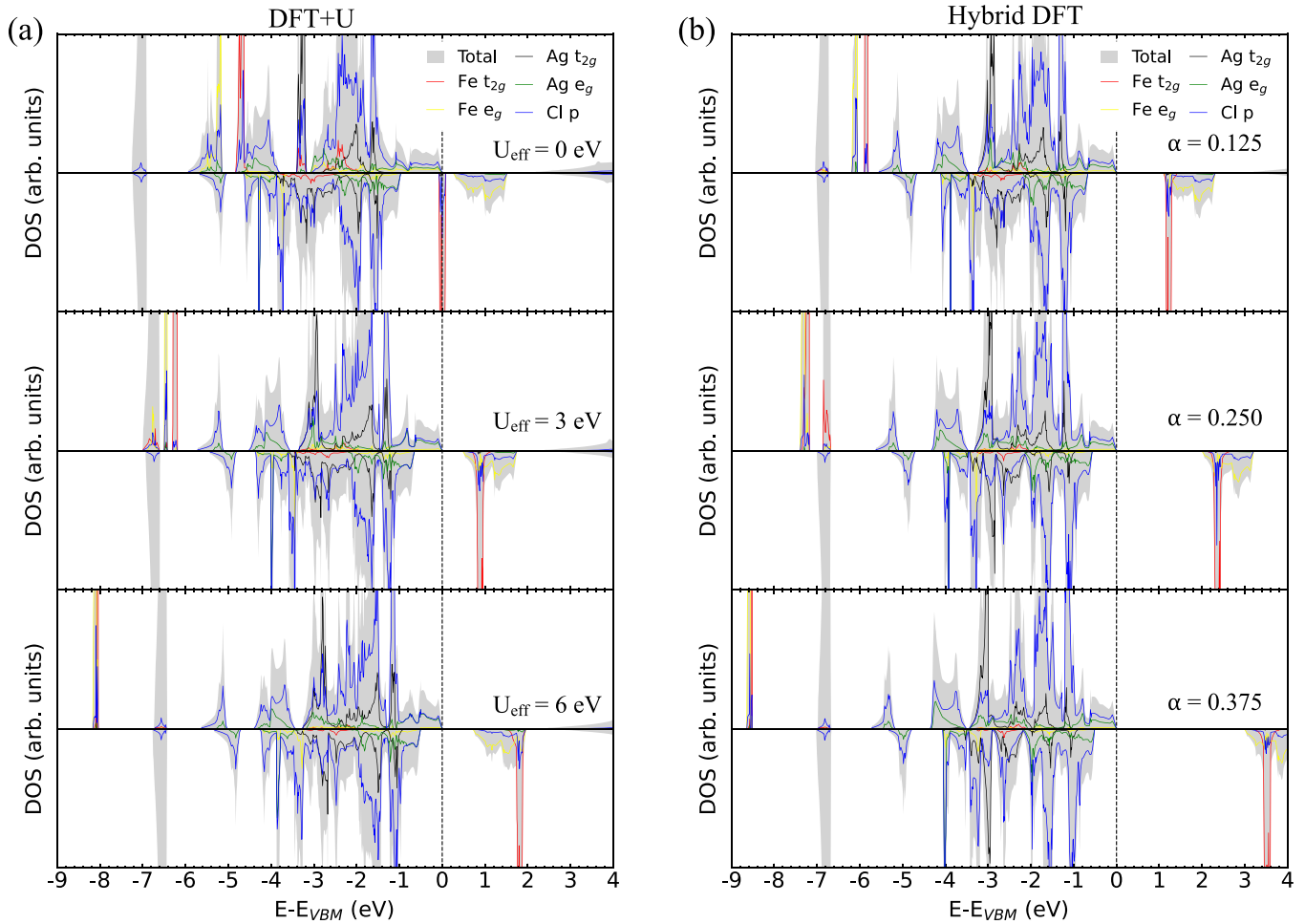|	ΔE (meV/f.u.)	
Magnetic state	$Cs_2NaFeCl_6$	$Cs_2AgFeCl_6$
FM	0	0
AFM-I	-8	-62
AFM-II	-6	-51
AFM-III	-8	-64
PM	-6	-50

FIG. 5. Electronic DOS for $Cs_2AgFeCl_6$ in the FM state, for (a) varying values of U on the Fe(d) states in the PBEsol $+ U$ methodology and (b) varying values of α in the hybrid DFT (default HSE06 range separation parameter). The DOS are aligned to the VBM. The unmarked peak at around -7 eV corresponds to Cs(p) states.

difference between the different AFM configurations (AFM-I and AFM-III, in particular) is, however, very small and likely smaller than the accuracy of our DFT simulations. We thus cannot assign a particular AFM configuration as the ground state. Furthermore, as pointed out in Ref. [8], the Fe atoms sit on an geometrically frustrated fcc lattice and it is thus likely that the true magnetic ground state is noncollinear. Such treatment is beyond the scope of the present work, but we encourage future studies to investigate this point.

For $Cs_2NaFeCl_6$, the energies across all spin configurations are close to degenerate on the accuracy in our calculations, indicating a weak interaction between Fe magnetic moments in this system. This is in agreement with the very low experimental Neél temperature of ~ 3 K.

For $Cs_2AgFeCl_6$, the energy differences across the spin configurations are larger, but the AFM-PM energy difference is still rather small, again in agreement with a low Neél temperature of ~ 18 K. The energy difference between the AFM/PM and the FM state is however much larger in $Cs_2AgFeCl_6$ compared to $Cs_2NaFeCl_6$, indicating some significant interaction between Fe magnetic moments. This is likely, as mentioned in Ref. [8], due to the covalent Ag(d)-Cl(p) interaction which can mediate the magnetic in-

teractions between the Fe spins to a larger degree than the mostly inert Na ion. A detailed study into the magnetic interactions in magnetic halide double perovskites is beyond the scope of the present work and will be reported elsewhere.

Figure 6 shows the DOS of $Cs_2NaFeCl_6$ and $Cs_2AgFeCl_6$ in their AFM-I spin configuration. While these DOS are qualitatively similar to their FM counterparts, there are some quantitative difference. In particular, the bandwidth of the e_g states is smaller in the AFM-I configuration, resulting in a somewhat smaller bandgap, in particular in the case of $Cs_2AgFeCl_6$.

Since the Neél temperatures of $Cs_2(Ag, Na)FeCl_6$ are low, the relevant magnetic setting for any prospective applications at or around ambient temperature is the PM phase. To model the electronic band structure in the PM state we employ a DLM spin configuration and then use the band unfolding formalism [29] to unfold the resulting band structure, yielding an effective band structure (EBS) in the primitive BZ of the double perovskite structure. The results are shown in Fig. 7 for $Cs_2NaFeCl_6$ and $Cs_2AgFeCl_6$, where we compare these EBSs to their corresponding band structures in the FM state.

We see that for $Cs_2NaFeCl_6$ the band structure is rather weakly affected by the different local spin environments that

(a)

(b)

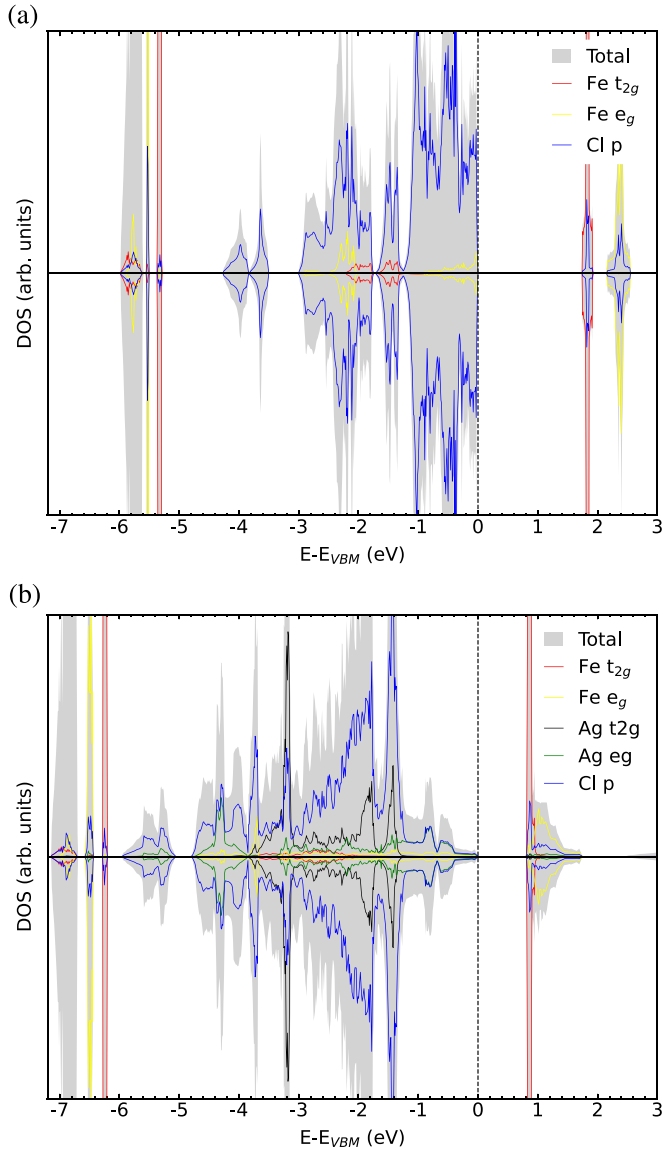

FIG. 6. Electronic DOS for (a) $Cs_2NaFeCl_6$ and (b) $Cs_2AgFeCl_6$ in their AFM-I spin configuration, calculated using PBEsol $+ U(3$ eV). The DOS are aligned to the VBM.

the Fe atoms experience and the EBS resembles the FM band structure quite closely, with minor shifts and broadening in certain bands with some Fe(e_g/t_{2g}) character.

The effects of the spin configuration on the band structure is significantly larger for $Cs_2AgFeCl_6$. First, we see that the PBEsol $+ U(3$ eV) bandgap is significantly increased in the PM as compared to the FM spin configuration. This follows from the decreased bandwidth in the PM state of the unoccupied Fe e_g band at the bottom of the conduction band and occupied Ag e_g band at the top of the valence band in the $\Gamma - X$ direction. This is a result of the weaker Fe-Fe interaction in this direction upon introduction of magnetic disorder and is present, although to a lesser extent, also for the unoccupied Fe e_g band in $Cs_2NaFeCl_6$.

Indeed, for $Cs_2AgFeCl_6$, all the states within ~1 eV of the valence band maximum, of Ag(e_g)+Cl(p) character are rather heavily broadened and shifted in the EBS as a result of the

disordered spin configuration on the Fe ions. This indicates that the bands of Ag(e_g) character are significantly influenced by the spin configuration of the neighboring Fe ions. This in turn suggests a stronger interaction between Fe spins, mediated by Ag(e_g) orbitals, which explains the larger energy difference between the FM and AFM spin configurations in $Cs_2AgFeCl_6$ compared to $Cs_2NaFeCl_6$.

It is important to note that broadening effects in the EBS may converge quite slowly with the size of the employed supercell [35]. Unfortunately, the computational complexity of employing larger supercells than the 640 atom ones used in this work is prohibitively large. Nevertheless, the presented result should be qualitatively accurate in terms of which states are effected by the disordered magnetism.

Analyzing the band structures of $Cs_2AgFeCl_6$ and $Cs_2NaFeCl_6$ for $U_{eff} = 3$ eV in their FM states, we find that for spin-allowed transitions, $Cs_2AgFeCl_6$ is an indirect bandgap semiconductor in the minority spin channel, with the VBM and CBM at the L and X points, respectively. $Cs_2NaFeCl_6$ is also an indirect semiconductor with VBM and CBM at the Γ and X points, respectively, due to the almost dispersionless $\Gamma - X$ branch at the top of the valence band, the direct bandgap is very close to the fundamental gap.

In the DLM state, where the two spin channels are equivalent, both $Cs_2AgFeCl_6$ and $Cs_2NaFeCl_6$ are practically direct band gap systems due to their flat Γ-X branches in the VB and the CBM at the X point.

IV. DISCUSSION

We now provide some thoughts regarding the choice of α and U_{eff}. As we have seen, basic structural properties are not strongly affected by these parameters, whereas the electronic structure is. It might therefore be tempting to attempt to tune U_{eff} or α to match the room temperature experimental bandgap values, 2.07–2.2 eV [13,36] and 1.55–1.6 eV [4,6], for $Cs_2NaFeCl_6$ and $Cs_2AgFeCl_6$. As can be judged from Figs. 2 and 5, this is possible for both $Cs_2NaFeCl_6$ and $Cs_2AgFeCl_6$ in the hybrid DFT framework, and also for $Cs_2NaFeCl_6$ in the PBEsol $+ U$ framework. We note, however, that this is rather precarious since, as has been mentioned above, varying U_{eff} or α has multiple consequences, for instance in regards to the amount of Fe(d) contribution at the top of the valence band.

In modeling the PM state we have chosen to use a U_{eff} value of 3 eV, since this gives the same ordering of the unoccupied e_g/t_{2g} states as hybrid DFT for reasonable values of α. The ordering of these states is indeed potentially important for, e.g., the transport properties of these systems since they provide very different effective electron masses. Indeed, the t_{2g} states are very flat, while the e_g bands have some curvature, corresponding to lower effective electron masses.

As the recent interest for $Cs_2AgFeCl_6$ and $Cs_2NaFeCl_6$ have emerged in the context of their membership of the lead-free halide double perovskite class of materials, it is instructive to point out similarities and differences of their electronic structure to some prototypical members of this class. The two prototypical members of this class are $Cs_2AgInCl_6$ and $Cs_2AgBi(Br/Cl)_6$. Indeed, these systems both have relatively disperse conduction bands, very different from the highly
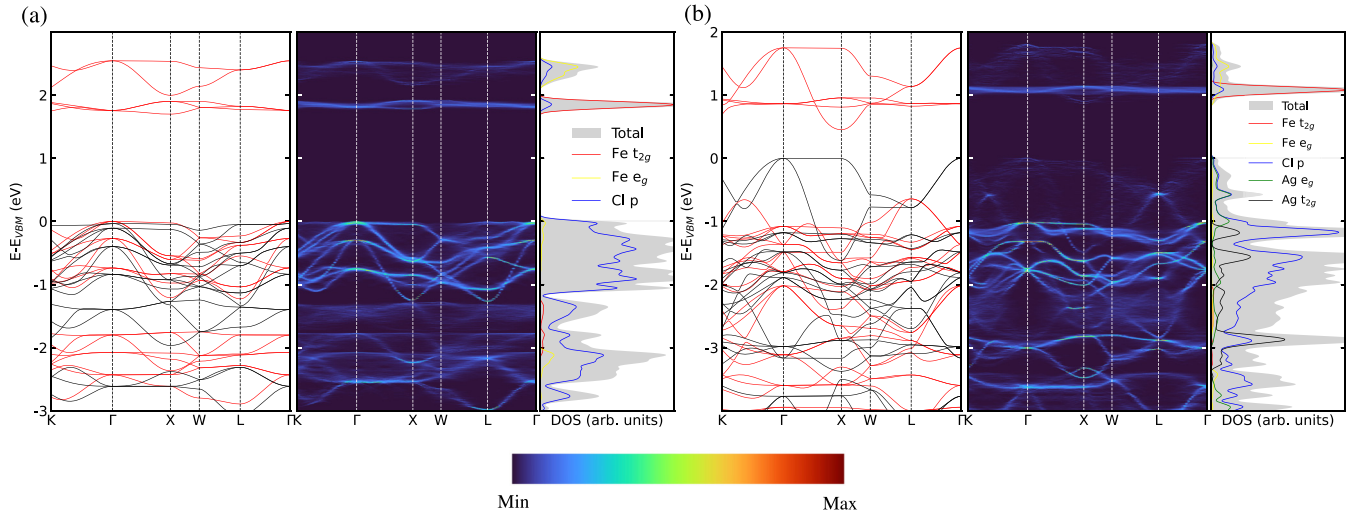
FIG. 7. Effective band structure (EBS) of (a) $Cs_2NaFeCl_6$ and (b) $Cs_2AgFeCl_6$ in DLM state. The left panels shows the band structure in the FM state for comparison, with the majority and minority spin bands in black and red, respectively. The right panels display the DOS in the DLM state. The intensity of the colorscale is capped at a third of the max value of the EBS to aid visualization.

localized Fe(d)-based states of, $Cs_2NaFeCl_6$ in particular. A possible implication of this is the self-localization of excess electrons, i.e., the formation of small-electron polarons on Fe^{3+} lattice sites. Initial exploratory calculations (not shown) indeed indicate that electron polaron formation is likely, but a comprehensive investigation into this topic is beyond the scope of this paper and is the subject of intended future work.

As has been mentioned throughout the paper, the presence of HS Fe^{3+} have implications in regards to the computational techniques that have to be used in order to accurately model these systems. Indeed, we have demonstrated that careful considerations regarding the magnetic state and strong correlation effects have to be made in order for accurate results to be obtained. Such considerations are not normally required in modeling systems within the class of halide perovskites.

V. CONCLUSION

To conclude, we have studied the electronic structure of Fe^{3+} containing double halide perovskites $Cs_2NaFeCl_6$ and $Cs_2AgFeCl_6$. We have investigated the impact of varying the effective on-site Hubbard interaction, U_{eff}, in DFT $+ U$ and the impact of the fraction of exact exchange, α, in the hybrid-DFT framework. We find that while basic structural properties are relatively insensitive to the choice of U_{eff} or α, several details of the electronic structure vary strongly. In particular, we find a set of highly localized Fe(d) states in the electronic structure of both $Cs_2NaFeCl_6$ and $Cs_2AgFeCl_6$, which vary sensitively with U_{eff} and α. A value of $U_{eff} = 3$ eV in DFT $+ U$ yields the same ordering of the Fe t_{2g} and e_g states as in hybrid-DFT, for reasonable values of α.

We have further investigated the impact of the magnetic state of these compounds. We find both systems to be antiferromagnetic at low T, but with rather small energy difference across different magnetic orderings. This is in agreement with the rather low experimental Neél temperatures of 3 K and 18 K for $Cs_2NaFeCl_6$ and $Cs_2AgFeCl_6$, respectively [8]. Furthermore, we have revealed the effect of disordered magnetism on the electronic band structures of these systems, finding that while $Cs_2NaFeCl_6$ is only weakly affected, $Cs_2AgFeCl_6$ is substantially influenced by the disordered magnetic state.

[1] A. K. Jena, A. Kulkarni, and T. Miyasaka, Halide perovskite photovoltaics: Background, status, and future prospects, Chem. Rev. **119**, 3036 (2019).

[2] W. Ning and F. Gao, Structural and functional diversity in lead-free halide perovskite materials, Adv. Mater. **31**, 1900326 (2019).

[3] F. Igbari, Z.-K. Wang, and L.-S. Liao, Progress of lead-free halide double perovskites, Adv. Energy Mater. **9**, 1803150 (2019).

[4] H. Yin, Y. Xian, Y. Zhang, W. Chen, X. Wen, N. U. Rahman, Y. Long, B. Jia, J. Fan, and W. Li, An emerging lead-free double-perovskite $Cs_2AgFeCl_6$: In single crystal, Adv. Funct. Mater. **30**, 2002225 (2020).

[5] W. Li, N. U. Rahman, Y. Xian, H. Yin, Y. Bao, Y. Long, S. Yuan, Y. Zhang, Y. Yuan, and J. Fan, Regulation of the order-disorder phase transition in a $Cs_2NaFeCl_6$ double perovskite towards reversible thermochromic application, J. Semicond. **42**, 072202 (2021).

[6] F. Ji, F. Wang, L. Kobera, S. Abbrent, J. Brus, W. Ning, and F. Gao, The atomic-level structure of bandgap engineered double perovskite alloys $Cs_2AgIn_{1-x}Fe_xCl_6$, Chem. Sci. **12**, 1730 (2021).

[7] J. Pebler, K. Schmidt, R. Haegele, and D. Babel, Untersuchung des MÖSSBAUER-effekts in elpasolithen $A_2'NaFeF_6$, Z. Naturforsch., B **31**, 1039 (1976).

[8] J. Xue, Z. Wang, A. Comstock, Z. Wang, H. H. Y. Sung, I. D. Williams, D. Sun, J. Liu, and H. Lu, Chemical control of magnetic ordering in hybrid Fe-Cl layered double perovskites, Chem. Mater. **34**, 2813 (2022).

[9] B. Himmetoglu, A. Floris, S. de Gironcoli, and M. Cococcioni, Hubbard-corrected DFT energy functionals: The LDA+U description of correlated systems, Int. J. Quantum Chem. **114**, 14 (2014).

[10] M. Cococcioni and S. de Gironcoli, Linear response approach to the calculation of the effective interaction parameters in the LDA + U method, Phys. Rev. B **71**, 035105 (2005).

[11] V. Ivády, R. Armiento, K. Szász, E. Janzén, A. Gali, and I. A. Abrikosov, Theoretical unification of hybrid-DFT and DFT + U methods for the treatment of localized orbitals, Phys. Rev. B **90**, 035146 (2014).

[12] B. Alling, T. Marten, and I. A. Abrikosov, Questionable collapse of the bulk modulus in CrN, Nat. Mater. **9**, 283 (2010).

[13] Y. Xian, H. Yin, Y. Bao, Y. Xiao, S. Yuan, N. U. Rahman, Y. Yuan, Y. Zhang, X. Meng, S. Jin, W. Li, and J. Fan, Engineered Electronic Structure and Carrier Dynamics in Emerging $Cs_2Ag_xNa_{1-x}FeCl_6$ Perovskite Single Crystals, J. Phys. Chem. Lett. **11**, 9535 (2020).

[14] K. Radja, B. L. Farah, A. Ibrahim, D. Lamia, I. Fatima, B. Nabil, A. Mohamed, Y. Al-Douri, and A. A. El-Rehim, Investigation of structural, magneto-electronic, elastic, mechanical and thermoelectric properties of novel lead-free halide double perovskite $Cs_2AgFeCl_6$: First-principles calcuations, J. Phys. Chem. Solids **167**, 110795 (2022).

[15] B. L. Gyorffy, A. J. Pindor, J. Staunton, G. M. Stocks, and H. Winter, A first-principles theory of ferromagnetic phase transitions in metals, J. Phys. F **15**, 1337 (1985).

[16] B. Alling, T. Marten, and I. A. Abrikosov, Effect of magnetic disorder and strong electron correlations on the thermodynamics of CrN, Phys. Rev. B **82**, 184430 (2010).

[17] P. E. Blöchl, Projector augmented-wave method, Phys. Rev. B **50**, 17953 (1994).

[18] G. Kresse and J. Furthmüller, Efficiency of *ab-initio* total energy calculations for metals and semiconductors using a plane-wave basis set, Comput. Mater. Sci. **6**, 15 (1996).

[19] G. Kresse and J. Furthmüller, Efficient iterative schemes for *ab initio* total-energy calculations using a plane-wave basis set, Phys. Rev. B **54**, 11169 (1996).

[20] G. Kresse and D. Joubert, From ultrasoft pseudopotentials to the projector augmented-wave method, Phys. Rev. B **59**, 1758 (1999).

[21] J. P. Perdew, A. Ruzsinszky, G. I. Csonka, O. A. Vydrov, G. E. Scuseria, L. A. Constantin, X. Zhou, and K. Burke, Restoring the Density-Gradient Expansion for Exchange in Solids and Surfaces, Phys. Rev. Lett. **100**, 136406 (2008).

[22] S. L. Dudarev, G. A. Botton, S. Y. Savrasov, C. J. Humphreys, and A. P. Sutton, Electron-energy-loss spectra and the structural stability of nickel oxide: An LSDA+U study, Phys. Rev. B **57**, 1505 (1998).

[23] A. V. Krukau, O. A. Vydrov, A. F. Izmaylov, and G. E. Scuseria, Influence of the exchange screening parameter on the performance of screened hybrid functionals, J. Chem. Phys. **125**, 224106 (2006).

[24] R. Dronskowski and P. E. Bloechl, Crystal orbital Hamilton populations (COHP): Energy-resolved visualization of chemical bonding in solids based on density-functional calculations, J. Phys. Chem. **97**, 8617 (1993).

[25] V. L. Deringer, A. L. Tchougréeff, and R. Dronskowski, Crystal orbital Hamilton population (COHP) analysis as projected from plane-wave basis sets, J. Phys. Chem. A **115**, 5461 (2011).

[26] S. Maintz, V. L. Deringer, A. L. Tchougréeff, and R. Dronskowski, Analytic projection from plane-wave and PAW wavefunctions and application to chemical-bonding analysis in solids, J. Comput. Chem. **34**, 2557 (2013).

[27] R. Nelson, C. Ertural, J. George, V. L. Deringer, G. Hautier, and R. Dronskowski, LOBSTER: Local orbital projections, atomic charges, and chemical-bonding analysis from projector-augmented-wave-based density-functional theory, J. Comput. Chem. **41**, 1931 (2020).

[28] A. Zunger, S.-H. Wei, L. G. Ferreira, and J. E. Bernard, Special Quasirandom Structures, Phys. Rev. Lett. **65**, 353 (1990).

[29] V. Popescu and A. Zunger, Extracting E versus $\vec{k}$ effective band structure from supercell calculations on alloys and impurities, Phys. Rev. B **85**, 085201 (2012).

[30] P. V. C. Medeiros, S. Stafström, and J. Björk, Effects of extrinsic and intrinsic perturbations on the electronic structure of graphene: Retaining an effective primitive cell band structure by band unfolding, Phys. Rev. B **89**, 041407(R) (2014).

[31] Using the default radius around the Fe atoms (RWIGS), as supplied by the VASP PAW potentials

[32] Q. Zhao and H. J. Kulik, Where does the density localize in the solid state? Divergent behavior for hybrids and DFT + U, J. Chem. Theory Comput. **14**, 670 (2018).

[33] A. V. Ushakov, S. V. Streltsov, and D. I. Khomskii, Crystal field splitting in correlated systems with negative charge-transfer gap, J. Phys.: Condens. Matter **23**, 445601 (2011).

[34] The three AFM-I, AFM-II and AFM-III configurations are defined eg. in Ref. [37].

[35] Z. Wang, O. I. Malyi, X. Zhao, and A. Zunger, Mass enhancement in 3d and $s - p$ perovskites from symmetry breaking, Phys. Rev. B **103**, 165110 (2021).

[36] F. Ji, *et al.* (unpublished).

[37] N.-N. Sun and H.-Y. Wang, The J_1-J_2 model on the face-centered-cubic lattices, J. Magn. Magn. Mater. **454**, 176 (2018).